# On the Advantages of Symmetrical Over Asymmetrical Multiphase AC Drives with Even Phase Number Using Direct Controllers

A. Gonzalez-Prieto, I. Gonzalez-Prieto, A. G. Yepes, *Senior Member, IEEE,*
M. J. Duran and J. Doval-Gandoy, *Member, IEEE*

***Abstract*— Multiphase electric drives offer attractive advantages over conventional three-phase systems. Some of the benefits are shared by all multiphase configurations, but the performance can be highly affected by the specific location of the stator windings. While the asymmetrical configuration has been traditionally a popular choice, the symmetrical disposition in even-phase machines has a main advantage: it is possible to generate $\alpha$-$\beta$ voltages without any contribution in different $x$-$y$ subspaces. This work explains and demonstrates this feature for the general case of distributed-winding symmetrical $n$-phase machines, with $n$ being an even number. Fortunately, direct controllers can benefit from this characteristic by exclusively selecting voltage states with only $\alpha$-$\beta$ voltage production. To illustrate this capability, a finite-control-set model predictive control (FCS-MPC) using these special voltage states is also suggested in this work for symmetrical six-phase electric drives. This approach provides a greater simplicity and much less current distortion than in standard FCS-MPC for the asymmetrical configuration. Comparative experimental results confirm the minimal $x$-$y$ injection of symmetrical configurations thanks to the proposed control actions (i.e., voltage states).**

***Index Terms*— Direct controllers, harmonic distortion, model predictive control, multiphase electric drives, stator winding arrangement.**

## I. INTRODUCTION

Three-phase electric machines have been the mainstream option for variable-speed drives in the last decades thanks to their suitable performance, low maintenance and high degree of development of the three-phase technology [1]. However, the requirements imposed on the next generation of electric drives have been further increased with the appearance of more-electric applications such as electric vehicles or wind energy systems, to name a few [2]. In this scenario, multiphase electric drives appear as a convenient alternative to three-phase systems, particularly in applications where a higher reliability and a better power distribution (lower phase current) are sought. Multiphase drives provide a higher post-fault tolerance without extra hardware, a better power distribution and extra freedom degrees to implement additional operating modes [2-3].

The use of multiple sets of three-phase windings has been the preferred option at industry in order to exploit the three-phase voltage source converter (VSC) technology [4-6]. Among this group, the six-phase option has noticeably awakened the interest of the research community [7-14]. According to the stator winding shifting, six-phase electric drives are classified into two main groups: asymmetrical (A6) [7-10] and symmetrical (S6) [11-13] configurations. The convenience of using one sort of winding disposition or the other has been discussed in the literature from different perspectives. For instance, [14] analyzed the performance of these electric motors when the machine is fed in a pulse-step mode. Simulation results from [14] showed that the asymmetrical configuration provided lower torque pulsations than its symmetrical counterpart. Presumably for this reason the use of A6 machines became popular and a high number of subsequent works adopted this type of winding disposition [15]. However, these torque pulsations in symmetrical machines were later mitigated with the application of numerous switching states per fundamental period, and as a result, the advantage of asymmetrical configurations was no longer than clear [15]. Since the use of several control actions per fundamental period is a common trend in modern regulation techniques [2-3], the symmetrical shifting cannot be discarded as an interesting six-phase alternative. Using a different approach, [16] recently analyzed the effect of winding configurations on six-phase induction machine (IM) parameters, but the VSC was neglected. On the other hand, the post-fault capability of different six-phase electric machines was performed in [17], evaluating their post-fault performance and derating for different open-phase fault scenarios. On the other hand, direct controllers, which directly switch the VSC state without pulse-width-modulation stage (e.g., FCS-MPC), are of significant interest in multiphase drives due to, e.g., their fast reference tracking [4]. The available control actions (VSC output voltages) for these controllers depend to a great extent on the drive type: however, based on the available studies comparing symmetrical and asymmetrical drives [15-17], the most convenient winding disposition for direct controllers is still to be established.

In order to provide a broader picture in the comparison between asymmetrical over symmetrical configurations, the analysis is approached hereafter from the point of view of the

Manuscript received February 2, 2021; revised April 3, 2021, May 2, 2021, and July 24, 2020; accepted July 29, 2021.

This research was funded in part by the Spanish Government under the Plan Estatal 2017-2020 with the reference RTI2018-096151-B-I00, in part by the Government of Galicia under the grant ED431F 2020/07, in part by the Ministry of Science, Innovation and Universities under the Ramon y Cajal grant RYC2018-024407-I, and in part by the Spanish State Research Agency (AEI) under project PID2019- 105612RB-I00/AEI/10.13039/501100011033.

A. Gonzalez-Prieto, I. Gonzalez-Prieto and M.J. Duran are with the Department of Electrical Engineering at the University of Malaga, Spain, e-mail: anggonpri@uma.es, igp@uma.es and mjduran@uma.es.

A. G. Yepes and J. Doval-Gandoy are with CINTECX, Universidade de Vigo, Applied Power Electronics Technology research group (APET), 36310 Vigo, Spain, e-mail: agyepes@uvigo.es and jdoval@uvigo.es.

available control actions for direct controllers and their impact on the generation of parasitic $x$-$y$ currents in distributed-winding machines. An in-depth study from this perspective is still missing, and this work aims to fill this gap showing that the existence of some specific voltage vectors in symmetrical configurations could tip the scales in their favor. In fact, the symmetrical structure presents an important advantage from this point of view: there are some active voltage vectors with a null production in the $x$-$y$ plane, whereas in the asymmetrical solution the flux/torque production always provokes an unavoidable $x$-$y$ voltage injection [18]. Although the former fact can be seen in the analysis of voltage vectors presented in [11-13], the potential advantages it may imply for direct controllers have not been discussed nor exploited so far. The application of a single control action per sampling period (e.g., in standard FCS-MPC) cannot ensure a low harmonic injection in A6 machines [18-19]. On the basis of this limitation, the implicit modulators in FCS-MPC have been enhanced with the utilization of different sets of virtual voltage vectors (VVs) [18-21]. This strategy allows reducing the time harmonic distortion caused by the nature of control actions in this stator winding shifting [18-21]. With regard to the use of VVs, the role of large voltage vectors has been highlighted in several works [18-19], because they offer the better ratio between the flux/torque production and the consequent $x$-$y$ injection [19]. Regrettably, regardless of the selected VV technique, the switching frequency increases and therefore the total losses could also augment. It is fortunate however that in the case of S6 machine, the implementation of a virtual voltage technique can be omitted, thanks to the null production of the large voltage vectors in the secondary subspace, as shown here. This situation can promote the selection of the S6 machine if it is desired to exploit the potential advantages of FCS-MPC, such as an important flexibility to include constraints and a suitable dynamic response [22].

To evaluate and take advantage of the interesting behavior of symmetrical windings over asymmetrical ones for direct controllers, this work provides the following contributions.

1) Comparative analysis of the different control actions in A6 and S6 machines in order to select the most appropriate subset of VSC voltage outputs for the FCS-MPC.
2) Postulation of a simple but general guideline to identify the switching states that provide null $x$-$y$ voltage production in multiphase machines with symmetrical winding configuration (generalized for $n$- phase machines with $n$ being even).
3) Definition of a simplified version of the FCS-MPC using only the previously selected switching states and skipping the $x$-$y$ model of the machine.
4) Experimental comparison of the FCS-MPC performance in S6 and A6 machines.

A preliminary version of this work was presented in [23], but here very significant new content is added, including extensive experimental results, comparison with asymmetrical windings, comparison between the use of only large voltage vectors and of all voltage vectors, analysis of the 12-phase case and extension to other phase numbers.

This manuscript is structured as follows. Section II describes the impact of the stator winding shifting on the available control actions of multiphase electric drives. Section III develops the proposed MPC based on a specific subset of switching states. Section IV shows the experimental results that validate the goodness of symmetrical shifting over the asymmetrical one and, finally, Section V summarizes the main conclusions.

## II. Stator Winding Distribution and Voltages States in Multiphase Electric Drives

### A. A Stator Winding Distribution Using Vector Space Decomposition

As it is well-known, the electric drive equations can be expressed in phase variables. Nevertheless, vector space decomposition (VSD) has been extensively employed because it allows a better insight into the electric drive behavior [24]. In fact, phase variables are expressed in a set of orthogonal subspaces with a physical meaning after VSD transformation. Namely, the $\alpha$-$\beta$ subspace is related with the flux/torque production, whereas the $x$-$y$ subspaces only produce stator copper losses in distributed-winding machines. Different harmonic components are projected into these orthogonal subspaces depending on the phase number and the stator winding shifting of each electric machine [25]. Focussing on the case of six-phase IM, asymmetrical and symmetrical configurations (Fig. 1) present different natures. Diverse harmonic components appear in the available orthogonal subspaces based on the selected stator shifting. For example, the 5th harmonic is mapped into the secondary subspace ($x$ - $y$ plane) for A6 machines, but into the $\alpha$-$\beta$ plane for S6 motors, where the 2nd harmonic is the lowest order in the $x$ – $y$ plane [25]. Considering this issue, different versions of the VSD transformation are necessary for each six-phase IM [25]:

$$[C_a]=\begin{bmatrix}\alpha\\ \beta\\ x\\ y\\ 0_+\\ 0_-\end{bmatrix}\left\{\frac{1}{3}\overbrace{\begin{bmatrix}1 & -1/2 & -1/2 & \sqrt{3}/2 & -\sqrt{3}/2 & 0\\ 0 & \sqrt{3}/2 & -\sqrt{3}/2 & 1/2 & 1/2 & -1\\ 1 & -1/2 & -1/2 & -\sqrt{3}/2 & \sqrt{3}/2 & 0\\ 0 & -\sqrt{3}/2 & \sqrt{3}/2 & 1/2 & 1/2 & -1\\ 1 & 1 & 1 & 0 & 0 & 0\\ 0 & 0 & 0 & 1 & 1 & 1\end{bmatrix}}^{[a_1\ b_1\ c_1\ a_2\ b_2\ c_2]}\right., \tag{1}$$

$$[C_s]=\begin{bmatrix}\alpha\\ \beta\\ x\\ y\\ 0_+\\ 0_-\end{bmatrix}\left\{\frac{1}{3}\overbrace{\begin{bmatrix}1 & -1/2 & -1/2 & 1/2 & -1 & 1/2\\ 0 & \sqrt{3}/2 & -\sqrt{3}/2 & \sqrt{3}/2 & 0 & -\sqrt{3}/2\\ 1 & -1/2 & -1/2 & -1/2 & 1 & -1/2\\ 0 & -\sqrt{3}/2 & \sqrt{3}/2 & \sqrt{3}/2 & 0 & -\sqrt{3}/2\\ 1 & 1 & 1 & 0 & 0 & 0\\ 0 & 0 & 0 & 1 & 1 & 1\end{bmatrix}}^{[a_1\ b_1\ c_1\ a_2\ b_2\ c_2]}\right. . \tag{2}$$

Being $[C_a]$ and $[C_s]$ the amplitude-invariant Clarke transformation for A6 and S6 machines, respectively. Additionally, this work assumes that space harmonic components can be neglected because the drive operates with a distributed-winding machine.

From (1)-(2) it is possible to represent the individual contribution of specific phase variables by taking the corresponding matrix elements either for $\alpha$-$\beta$ or $x$-$y$ planes. For the sake of example, let us consider a per unit amplitude in phase variable $a_2$. From (1), the $\alpha$-$\beta$ contribution in the

asymmetrical case is defined by the matrix elements $C_a[1,4]$ and $C_a[2,4]$, whereas the $x$-$y$ production can be quantified from $C_a[3,4]$ and $C_a[4,4]$, as it is depicted in Fig. 2. Similarly, it follows from (2) that the $\alpha$-$\beta$ contribution in the symmetrical case is based on the elements $[C_s][1,4]$ and $[C_s][2,4]$, whereas the elements $[C_s][3,4]$ and $[C_s][4,4]$ represent the $x$-$y$ contribution, as it is depicted in Fig. 3. Following the same procedure, the projections of all phases are obtained in Figs. 2 and 3.

It can be observed in Fig. 3 that the contribution of three $\alpha$ - $\beta$ adjacent phases always presents a favourable scenario in the secondary subspace, where a balanced three-phase system appears for S6 machines. Taking phases $a_1$, $a_2$ and $c_2$ as an example, it is shown in Fig. 3 with orange arrows that the vector sum of the contributions from these phases is null. This cancellation effect is not found in the A6 case (see Fig. 2), and unfortunately, this will have significant implications on the control actions that are available in direct controllers (addressed in Section III). The reader can verify that any three adjacent phases meet the rule that has been previously exemplified if S6 machines are considered. Although the previous explanation provides a geometric insight of the cancellation effect, this issue is further generalized and mathematically demonstrated in Section II-D.

### *B. Voltage States for Six-Phase Electric Drives*

Applying the amplitude-invariant Clarke transformation to the stator phase voltages, they can be expressed in VSD orthogonal subspaces. However, for that purpose, it is necessary to establish in a first step the phase voltages in the electric machine. First, a double three-phase two-level VSC feeding a six phase IM is considered. Therefore, the switching state $S_i$ of each VSC leg can be modeled as follows: $S_i = 1$ if the upper switch is ON and the lower switch is OFF, whereas $S_i = 0$ when the opposite situation occurs [18]. Therefore, the vector $[S] = [S_{a1}, S_{b1}, S_{c1}, S_{a2}, S_{b2}, S_{c2}]$, defined by the switching state of each VSC leg, and the dc-link voltage $V_{DC}$, allow the calculation of stator phase voltages $[v_s]$ independently from the winding configuration [18]:

$$\begin{bmatrix} v_{a1} \\ v_{b1} \\ v_{c1} \\ v_{a2} \\ v_{b2} \\ v_{c2} \end{bmatrix} = \frac{V_{DC}}{3} \cdot \begin{bmatrix} 2 & -1 & -1 & 0 & 0 & 0 \\ -1 & 2 & -1 & 0 & 0 & 0 \\ -1 & -1 & 2 & 0 & 0 & 0 \\ 0 & 0 & 0 & 2 & -1 & -1 \\ 0 & 0 & 0 & -1 & 2 & -1 \\ 0 & 0 & 0 & -1 & -1 & 2 \end{bmatrix} \cdot \begin{bmatrix} S_{a1} \\ S_{b1} \\ S_{c1} \\ S_{a2} \\ S_{b2} \\ S_{c2} \end{bmatrix}. \quad (3)$$

Then, the VSD transformation can be used to map $[v_s]$ into the different orthogonal subspaces:

$$\left[v^a_{\alpha s}\ v^a_{\beta s}\ v^a_{xs}\ v^a_{ys}\ v^a_{0+}\ v^a_{0-}\right]^{\mathrm{T}} = [C_a][v_{a1}\ v_{b1}\ v_{c1}\ v_{a2}\ v_{b2}\ v_{c2}]^{\mathrm{T}} \quad (4)$$

$$\left[v^s_{\alpha s}\ v^s_{\beta s}\ v^s_{xs}\ v^s_{ys}\ v^s_{0+}\ v^s_{0-}\right]^{\mathrm{T}} = [C_s][v_{a1}\ v_{b1}\ v_{c1}\ v_{a2}\ v_{b2}\ v_{c2}]^{\mathrm{T}}, \quad (5)$$

where the superscripts $a$ and $s$ indicate asymmetrical and symmetrical configurations, respectively. Zero-sequence components ($0_+$-$0_-$) are omitted from the analysis because their corresponding currents cannot flow when the two neutral points are isolated.

Focusing on the available voltage vectors in each winding shifting, Figs. 4 and 5 show the voltage vectors location for A6 and S6 drives, respectively. The voltage states in Figs. 4 and 5 have been identified with the decimal number equivalent to the binary codification of vector $[S]$. Regarding the voltage vector location in $\alpha$-$\beta$ and $x$-$y$ subspaces, the considered multiphase machines present control actions with a rather different nature. In the A6 configuration, all the $\alpha$-$\beta$ active voltage vectors cause a non-null voltage production in the secondary subspace, as expected from the vector decomposition of Fig. 2. On the contrary, in the symmetrical distribution some active voltage vectors provide a desirable null $x$-$y$ voltage generation. This opposite scenario is related to the vector decomposition in the $\alpha$-$\beta$ and $x$-$y$ subspaces in the studied multiphase machines, depicted in Fig. 3.

In order to exemplify the previous statement, the voltage vector $V_{37}$ is employed as a basis for the analysis. $V_{37}$ provides the maximum $\alpha$-$\beta$ voltage in the studied multiphase machines (64% of $V_{DC}$ in asymmetrical configuration and 66.7% of $V_{DC}$ in S6 machines). Founded on its $\alpha$-$\beta$ contribution, this switching state is defined as a large voltage vector [11,18]. Furthermore, this control action is generated with the same switching vector $[S]$ in both machines:

$$[S_{37}] = [1,0,0,1,0,1]. \quad (6)$$

The vectors related to the generation of $V_{37}$ are highlighted with orange arrows in Figs. 2 and 3. In the case of the asymmetrical distribution, the $x$-$y$ vector sum of active vectors of $V_{37}$ does not achieve a null value due to their specific decomposition in this subspace. Fortunately, this issue is solved in the symmetrical configuration, where the $x$-$y$ vector sum becomes zero. The active vectors happen to be in a balanced three-phase system in the secondary subspace, as previously exposed for phase variables (Section II-A). Indeed, this null harmonic injection occurs for all voltage vectors with three ON values in the switching vector $[S]$, if the three phases are adjacent in the $\alpha$-$\beta$ plane. These conditions are precisely satisfied by all large voltage vectors in S6 machines. Therefore, the symmetrical winding presents an important advantage to mitigate the time harmonic distortion over the asymmetrical disposition: the control designer can select large $\alpha$-$\beta$ vectors without exciting $x$-$y$, hence promoting current quality and efficiency, while preserving high dc-link utilization.

This advantageous situation is not exclusively found in S6 machines, where the control scheme can be simplified if these control actions are employed. Propitiously, large voltage

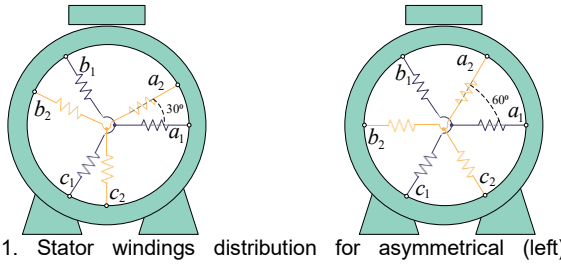


Fig. 1. Stator windings distribution for asymmetrical (left) and symmetrical (right) six-phase IM.

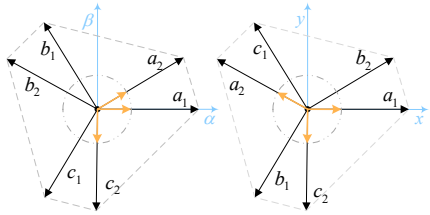


Fig. 2. Vector decomposition of the phase variables according to (1) in $\alpha$-$\beta$ (left) and $x$-$y$ subspaces (right) in an A6 IM.

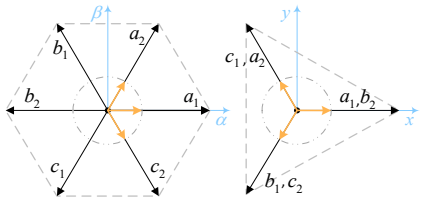


Fig. 3. Vector decomposition of the phase variables according to (2) in $\alpha$-$\beta$ (left) and $x$-$y$ subspaces (right) in a S6 IM.

vectors provide the complete mitigation of $x$-$y$ components for different symmetrical electric machines when the following requirements are fulfilled:

- R1. The number of stator phases is even.
- R2. The harmonic orders projected in the considered secondary subspace are even.

In addition, large voltage vectors present an interesting common feature for the aforementioned symmetrical electric drives (R1). This useful set of voltage states is always composed of ON values in $n/2$ adjacent stator phases, being $n$ the number of the stator phases. Therefore, this favorable subset of control actions can be identified in a trivial manner for $n$-phase multiphase machines that comply with R1.

### C. Large Voltage Vectors in Symmetrical Twelve-Phase Electric Drives

To confirm the assertions defined in the previous point, a symmetrical twelve-phase machine is considered as a case study. The number of phases is even (R1) and two out of the three $x-y$ subspaces fulfill R2. Fig. 6 shows the vector decomposition for the analyzed twelve-phase machine, obtained with the application of the corresponding VSD transformation [25-26]. For this IM, the lowest harmonic components in two out of the three secondary subspaces are 2nd and 4th harmonic order [25-26]; whereas in the other one 5th harmonic order appears as the lowest component order [25-26]. For the sake of example, the large voltage vector $V_{603}$ is employed in what follows. Fig. 7 shows the location of this control action (with a diamond) in the $\alpha$-$\beta$ plane. As expected, this voltage vector is defined by ON values in $n$/2=6 adjacent stator phases (Fig. 6):

$$[S_{603}] = [0,0,1,0,0,1,0,1,1,0,1,1], \quad (7)$$

where $[S] = [S_{a1}, S_{b1}, S_{c1}, S_{a2}, S_{b2}, S_{c2}, S_{a3}, S_{b3}, S_{c3}, S_{a4}, S_{b4}, S_{c4}]$.

Concerning the secondary contribution of the selected control action, the vector sum is null in the secondary subspaces, where harmonic orders are even, as shown in Fig. 6. These $x$-$y$ subspaces satisfy the R2 requirement and consequently their voltage contribution is non-existent. Unfortunately, the vector sum does not completely mitigate the harmonic injection in the third secondary subspace (Fig. 6), as a result of the vector decomposition caused by the projected harmonic components. Considering this voltage vector behavior, the symmetrical twelve-phase machine could be regulated like an asymmetrical six-phase machine if large voltage vectors are employed as active control actions. However, the suitable nature of large voltage vectors in symmetrical twelve-phase machine is not obtained in its asymmetrical counterpart [27], because odd harmonics are projected in the secondary subspaces [27]. A mathematical demonstration for a generic symmetrical $n$-phase case is included next for the sake of completeness.

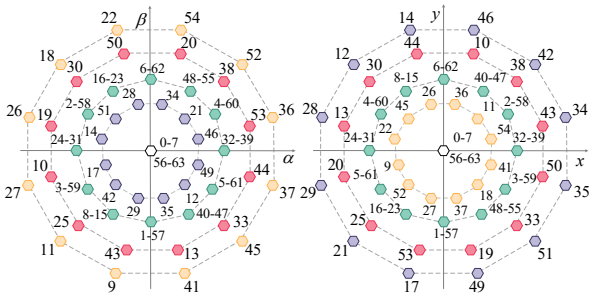


Fig. 4. Voltage vectors in $\alpha$-$\beta$ and $x$-$y$ subspaces for an A6 electric drive.

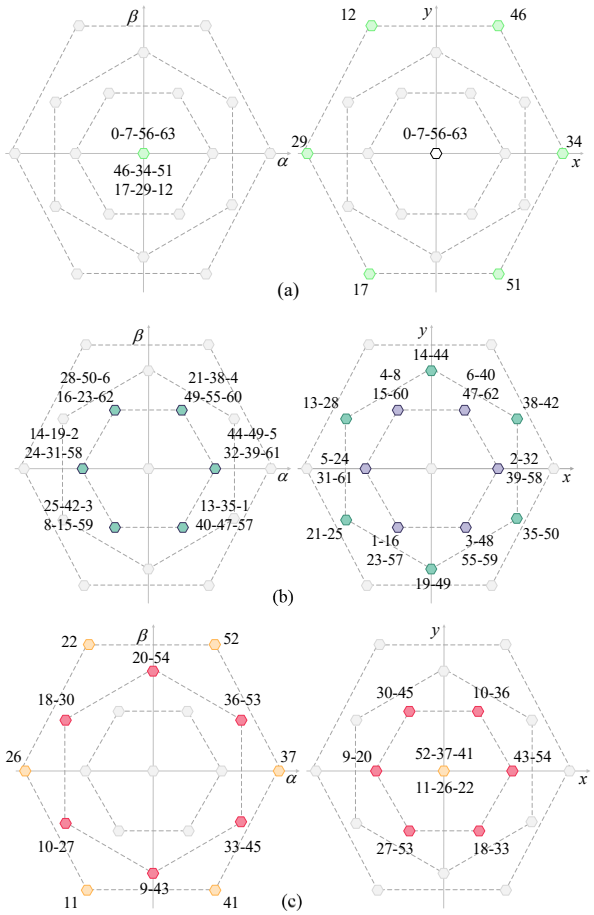


Fig. 5. Voltage vectors in $\alpha$-$\beta$ and $x$-$y$ subspaces for a S6 electric drive. From top to bottom: (a) null $\alpha$-$\beta$ and null voltage vectors, (b) small $\alpha$-$\beta$ voltage vectors and (c) large $\alpha$-$\beta$ and medium $\alpha$-$\beta$ voltage vectors.

### D. Mathematical Insight of Large Voltage Vectors Nature in Even Symmetrical Machines

Given an $n$-phase symmetrical machine, the stator phases are displaced by $2\pi/n$. Thus, considering complex-vector notation and even $n$, the projections of the instantaneous $p$th-phase ($p$=0,1,…$n$-1) voltage $v_p$ produced by the VSD into the $\alpha$ - $\beta$ and $x_\sigma$-$y_\sigma$ ($\sigma$ =2,3,…,$n$/2-1) planes are respectively

$$[v^p_{\alpha\beta}] = v_p e^{jp2\pi/n} \quad (8)$$

$$[v^p_{xy\sigma}] = v_p e^{j\sigma p2\pi/n}. \quad (9)$$

This corresponds to the vectors represented in Figs. 3 and 6 for the particular cases of symmetrical six- and twelve-phase machines.

As previously exposed, the large $\alpha$ - $\beta$ voltage vectors are those such that $S_i$ is 1 for $n$/2 consecutive phases (all of which

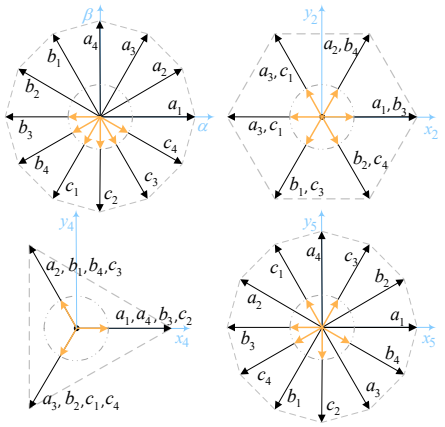


Fig. 6. Vector decomposition of the phase variables in $\alpha$-$\beta$ (up-left), $x_2$ - $y_2$ (up-right), $x_4$-$y_4$ (down-left) and $x_5$-$y_5$ (down-right) subspaces in a symmetrical twelve-phase IM.

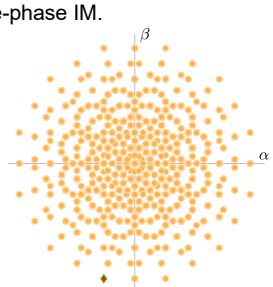


Fig. 7. Voltage vector location in $\alpha$-$\beta$ subspace for a symmetrical twelve-phase IM fed by a two-level VSC.

have positive contribution in the resulting vector direction) and 0 for the other $n/2$ ones (none of which do). Consequently, based on this fact, using (7) and considering that the $p$th-phase is the first one with $S_i$ =1, the resulting voltage vector in the $x_\sigma$ - $y_\sigma$ plane is

$$[v_{xy\sigma}] = v_p \sum_{m=p}^{p+\frac{n}{2}-1} e^{jm\sigma 2\pi/n} = v_p e^{jp\sigma 2\pi/n} \sum_{m=0}^{\frac{n}{2}-1} e^{jm\sigma 2\pi/n}. \quad (10)$$

At this point, it is worth remarking that $\sigma$ matches the lowest order of integer harmonic mapped into the $x_\sigma$-$y_\sigma$ plane [26]. If $\sigma$ is even, (10) can be rewritten as

$$[v_{xy\sigma}] = v_p e^{jp\sigma 2\pi/n} \sum_{m=0}^{n-1} e^{jm\sigma' 2\pi/n} \quad (11)$$

where $\sigma'$=$\sigma$ /2 is integer. In accordance with the Roots of Unity theory [26], it follows that the summation in (11), and hence the resulting $x_\sigma$-$y_\sigma$ voltage vector, is zero.

To sum up, large voltage vectors in symmetrical multiphase machines with even number of phases (R1) provide a null value in $x$-$y$ subspaces that satisfy R2. Based on this fact, this collection of easily identifiable voltage states can be defined as suitable control actions to mitigate the $x$-$y$ injection for direct controllers when requirements R1 and R2 are fulfilled.

## III. FCS-MPC Strategies

The previous voltage vector analysis can be used to develop different FCS-MPC approaches depending on the nature of the selectable control actions. With this in mind, this section describes two FCS-MPC schemes for the case study with six-phase machines. Standard FCS-MPC (termed FCS-MPC#1 from now on) retains the $x$-$y$ components in the control scheme. On the contrary, reduced FCS-MPC (termed FCS-MPC#2 from now on) makes use of the special features of large voltage vectors to avoid the use of $x$-$y$ components and simplify in this way the control stage. Both approaches possess nevertheless several similarities, as it is illustrated in Figs. 8 and 9. For example, both MPC techniques employ an outer proportional-integral (PI) controller to regulate the mechanical speed $\omega_m$ and two-stage inner predictive controllers to follow the stator current $i_s$. The inverse Park transformation matrix $[D]^{-1}$ [19] is employed to transform the reference $d$-$q$ currents $i^*_{dq}$ into the refence VSD currents $i^*_{\alpha\beta}$. Furthermore, regardless of the implemented FCS-MPC version, a single switching state $[S]$ per control cycle is applied. A further description of FCS-MPC#1 and #2 is provided next.

### A. Standard FCS-MPC (FCS-MPC#1)

This popular FCS-MPC [22] approach includes $\alpha$-$\beta$ and $x$-$y$ components in the discretized machine model since the selectable control actions cannot directly regulate the secondary subspace. Subsequently, the discretized machine model is

$$\frac{d}{dt}[X_{\alpha\beta xy}] = [A] \cdot [X_{\alpha\beta xy}] + [B] \cdot [V_{\alpha\beta xy}], \quad (12)$$

with

$$[V_{\alpha\beta xy}] = [v_{\alpha s}\ v_{\beta s}\ v_{xs}\ v_{ys}\ 0\ 0]^{\mathrm{T}}, [X_{\alpha\beta xy}] = [i_\alpha\ i_\beta\ i_x\ i_y\ \lambda_{\alpha r}\ \lambda_{\beta r}]$$

where $[A]$ and $[B]$ are obtained from the discretization of six-phase IM equations [18], and $\lambda_{\alpha\beta}$ and $i_{\alpha\beta xy}$ are the $\alpha$-$\beta$ magnetic rotor flux components and the VSD stator currents, respectively.

As shown in Fig. 8, the predictive machine model is employed in the two stages of the inner current control in order to estimate the predicted stator currents $\hat{\imath}_{\alpha\beta xy}$ produced by each voltage vector. According to this approach, the standard FCS-MPC is based on a two-step prediction horizon ($k$+2) and, consequently, the one-step delay compensation approach is inherently included in its scheme [22]. Finally, the predictive currents and the reference currents $i^*_{\alpha\beta xy}$ are evaluated in a predefined cost-function to select the better control action at each sampling period [19]:

$$J_1 = (i^*_\alpha - \hat{\imath}_\alpha)^2 + \left(i^*_\beta - \hat{\imath}_\beta\right)^2 + k_{xy} \cdot [(i^*_x - \hat{\imath}_x)^2 + \left(i^*_y - \hat{\imath}_y\right)^2]. \quad (13)$$

being $k_{xy}$ the weighting factor related to the $x$-$y$ regulation. The value of this parameter is tuned up to obtain a suitable flux/torque regulation and a mitigated $x$-$y$ production [19].

### B. Reduced FCS-MPC (FCS-MPC#2)

Using the special localization of large voltage vectors in S6 machines, a reduced FCS-MPC scheme can be employed if only this set of voltage states are defined as selectable active control actions. Voltage vectors with null production in $\alpha$-$\beta$ and $x$-$y$ planes, i.e., null voltage vectors (0, 7, 56, 63) in Fig. 5a, are also added as available switching states. This assumption is established since these switching states offer a null harmonic $x$-$y$ voltage injection (shown in Section II) and, consequently, $x$-$y$ currents are directly regulated (to zero) in open-loop mode. Exploiting this feature, $x$-$y$ currents can be omitted from the discretized machine model:

$$\frac{d}{dt}[X_{\alpha\beta}] = [\bar{A}] \cdot [X_{\alpha\beta}] + [\bar{B}] \cdot [V_{\alpha\beta}], \quad (14)$$

where

$$[V_{\alpha\beta}] = [v_{\alpha s}\ v_{\beta s}\ \ 0\ 0]^{\mathrm{T}}, [X_{\alpha\beta}] = [i_\alpha\ i_\beta\ \ \lambda_{\alpha r}\ \lambda_{\beta r}]^{\mathrm{T}}.$$

Matrices $[\bar{A}]$ and $[\bar{B}]$ depend on the machine parameters [28]. Although the regulation of $x$-$y$ components is carried out in open-loop mode, the impact of inverter non-linearities is small because the switching frequency for the target applications is relatively low.

The cost function can be defined using an analogous approach, and therefore, a simplified version of (9) can be established:

$$J_2 = (i_\alpha^* - \hat{\imath}_\alpha)^2 + \left(i_\beta^* - \hat{\imath}_\beta\right)^2, \tag{15}$$

where the $x$-$y$ weighting factor is not necessary anymore.

It is worth noting that the computational burden of this MPC version is minimized thanks to the assumptions employed in its building process.

The next section proves the impact of the stator winding shifting on the capability of the considered FCS-MPC schemes to achieve a lower harmonic distortion.

## IV. Experimental Validation

The experimental setup is shown in Fig. 10. The A6 and S6 induction motors are alternatively coupled to an eddy-current brake in a test bench. These two machines were obtained by rewinding the stator of two originally identical three-phase induction motors, with 24 stator slots and 18 rotor bars. Their main parameters, obtained from the method detailed in [29], are displayed in Table I. The six-phase inverter is built by combining two three-phase Semikron converter modules, based on insulated-gate bipolar transistors (IGBTs). The IGBT dead time is 3 μs. The dc-link voltage is kept at 700 V by a dc voltage source. The control is run with a sampling frequency of 10 kHz in a dSPACE-DS1006 platform.

Test 1 aims to highlight the importance of the $x$-$y$ components in the current control performance due to the lower value of their equivalent stator impedance [16]. For this purpose, two different versions of a standard FCS-MPC are assessed in the considered S6 motor. The first MPC option (FCS-MPC#1) is based on the use of all available voltage vectors as possible control actions (left plots in Fig. 11), whereas in the second MPC version (right plots in Fig. 11) only large and null voltage

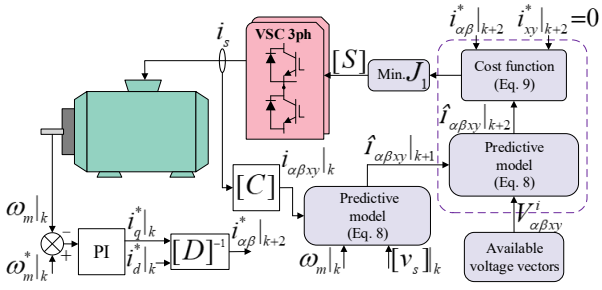


Fig. 8. Standard FCS-MPC (i.e., FCS-MPC#1) control scheme.

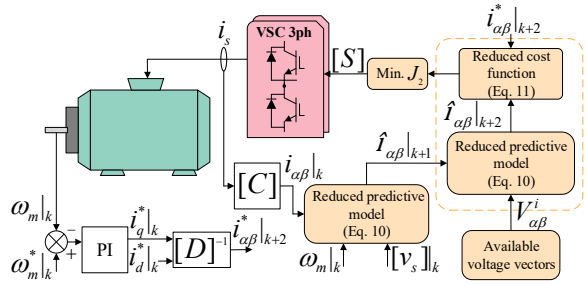


Fig. 9. Reduced FCS-MPC (i.e., FCS-MPC#2) control scheme.

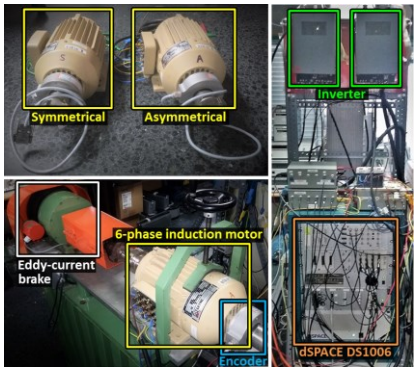


Fig. 10. Experimental setup.

vectors are defined as selectable switching states (FCS-MPC#2). The analyzed FCS-MPC alternatives achieve the tracking of the reference speed (Fig. 11a) with an acceptable regulation of the components related to the flux/torque production (Fig. 11b). Focusing on the secondary components (Fig. 11c), the scenario is completely different because the equivalent impedance of this orthogonal plane is much lower [16]. For this reason, the use of control actions with a null contribution in the $x$-$y$ subspace is vital to provide a suitable current quality. Even a rather low voltage injection can produce undesired large amplitude of harmonic currents. As a consequence of the aforementioned harmonic injection, the waveform of the phase currents $i_{a_1b_1c_1}$ shows unsought peaks (Fig. 11d) despite having a higher number of switching states in this control scheme (FCS-MPC#1). This better harmonic spectrum of the phase current waveform (Fig. 11f) has been obtained just increasing the average switching frequency $\bar{f}_{sw}$ by 2.35%, being $\bar{f}_{sw}$ equal to:

$$\bar{f}_{sw} = \left(f_{sw}^{a_1} + f_{sw}^{b_1} + f_{sw}^{a_1} + f_{sw}^{a_2} + f_{sw}^{b_2} + f_{sw}^{c_2}\right)/6\,, \tag{16}$$

where the switching frequency of each phase is calculated as follows:

$$f_{sw}^{a_1} = \frac{\sum_{i=0}^{m-1} |S_{a1}|_{i+1} - S_{a1}|_i|}{2 \cdot t_{test}} \tag{17}$$

being $m$ the amount of data of the specific test (500000) and $t_{test}$ the test duration (0.5 s). In addition to an improvement of the current quality, FCS-MPC#2 requires lower computational burden than the standard FCS-MPC#1.

Test 2 is proposed in order to extend the analysis of Test 1 to the A6 machine. For that purpose, high-speed conditions for the A6 induction machine are tested when FCS-MPC#1 uses all the available voltage vectors (left column of Fig. 12) and FCS-MPC#1 exclusively considers large voltage vectors (right column of Fig. 12). The tracking of the reference speed (2000 rpm) is satisfactorily done regardless of the implemented FCS-MPC approach. Focusing on the flux/torque regulation, the higher number of available switching states allows enhancing the $\alpha$-$\beta$ ripple (Fig. 12b). Unfortunately, the cost of this improvement in the plane related to the flux/torque production is an important injection of $x$-$y$ components (Fig. 12c) and consequently, a lower quality of phase currents, as shown in Fig. R2-2d. This situation appears because the impedance of the secondary $x$ - $y$ subspace is typically low in distributed-winding machines [16]. For this reason, the phase current quality becomes highly dependent on how the $x$ - $y$ current regulation is performed [19].

TABLE I
PARAMETERS OF SIX-PHASE INDUCTION MOTORS FOR THE EXPERIMENTS

| Parameter description | Asymmetrical | Symmetrical |
|---|---|---|
| Stator resistance (Ω) | 6.7 | 6.7 |
| Rotor resistance (Ω) | 5.3 | 5.0 |
| Stator leakage inductance (mH) | 5.2 | 4.6 |
| Rotor leakage inductance (mH) | 55.7 | 59.7 |
| Magnetizing inductance (mH) | 708.6 | 707.4 |
| Rated voltage (V) | 230 | 230 |
| Rated current (A) | 3.8 | 3.8 |
| Rated frequency (Hz) | 50 | 50 |
| Pole pairs | 1 | 1 |
| Stator slots | 24 | 24 |
| Rotor bars | 18 | 18 |

Test 3 illustrates, for a high-speed operating situation, the performance of the asymmetrical (left plots in Fig. 13, using FCS-MPC#1) and symmetrical (right plots in Fig. 13, using FCS-MPC#2) six-phase IM, when only large voltage vectors are considered for both cases as active switching states. Concerning the speed reference tracking, it is carried out in a satisfactory manner for both machines (Fig. 13a). Nevertheless, from the point of view of the current quality, two different scenarios appear depending on the analyzed six-phase motor. This result is specially affected by the contribution of the active voltage vectors in the secondary subspace of each IM (Figs. 4 and 5c). Thereby, although the $\alpha$-$\beta$ currents show sinusoidal waveform (Fig. 13b), the harmonic injection in the case of the A6 machine is significantly higher than in the symmetrical shifting (Fig. 13c and 13f). As a consequence of this $x$-$y$ production, the phase currents of the A6 machine present undesired harmonic distortion (see Fig. 13d). Fortunately, this situation is solved when the FCS-MPC#2 is implemented in the S6 IM thanks to the suitable performance of large voltage vectors in the secondary subspace. FCS-MPC#2 can achieve a reduced harmonic injection despite using a single switching state per sampling period. In addition, as in the case of the symmetrical machine regulated using FCS-MPC#2, the control action selection is only focused on the flux/torque regulation, hence a lower toque ripple is obtained (see Fig. 13e). Table II presents as quality indexes the average total harmonic distortion ($\overline{THD}$) and the average root mean square ($\overline{rms}$) of phase currents for this operating scenario. For the considered symmetrical distribution, the $\overline{THD}$ is 72.04% lower than in the asymmetrical machine for similar electric parameters (Table I). Additionally, Table II adds the usage level requirements for each specific operating point. The $\bar{f}_{sw}$ is directly influenced by the value of the null voltage vector usage. The transition from a null to a large voltage vector implies a higher number of VSC leg changes than in the case of two adjacent large voltage vectors or two null voltage vectors [28]. Therefore, the switching frequency can be characterized by the usage of the null voltage vector.

A low-speed scenario is explored in Test 4 for the studied A6 and S6 motors. In this third test, the speed/current regulation is again satisfactorily achieved using FCS-MPC#1 (A6) and

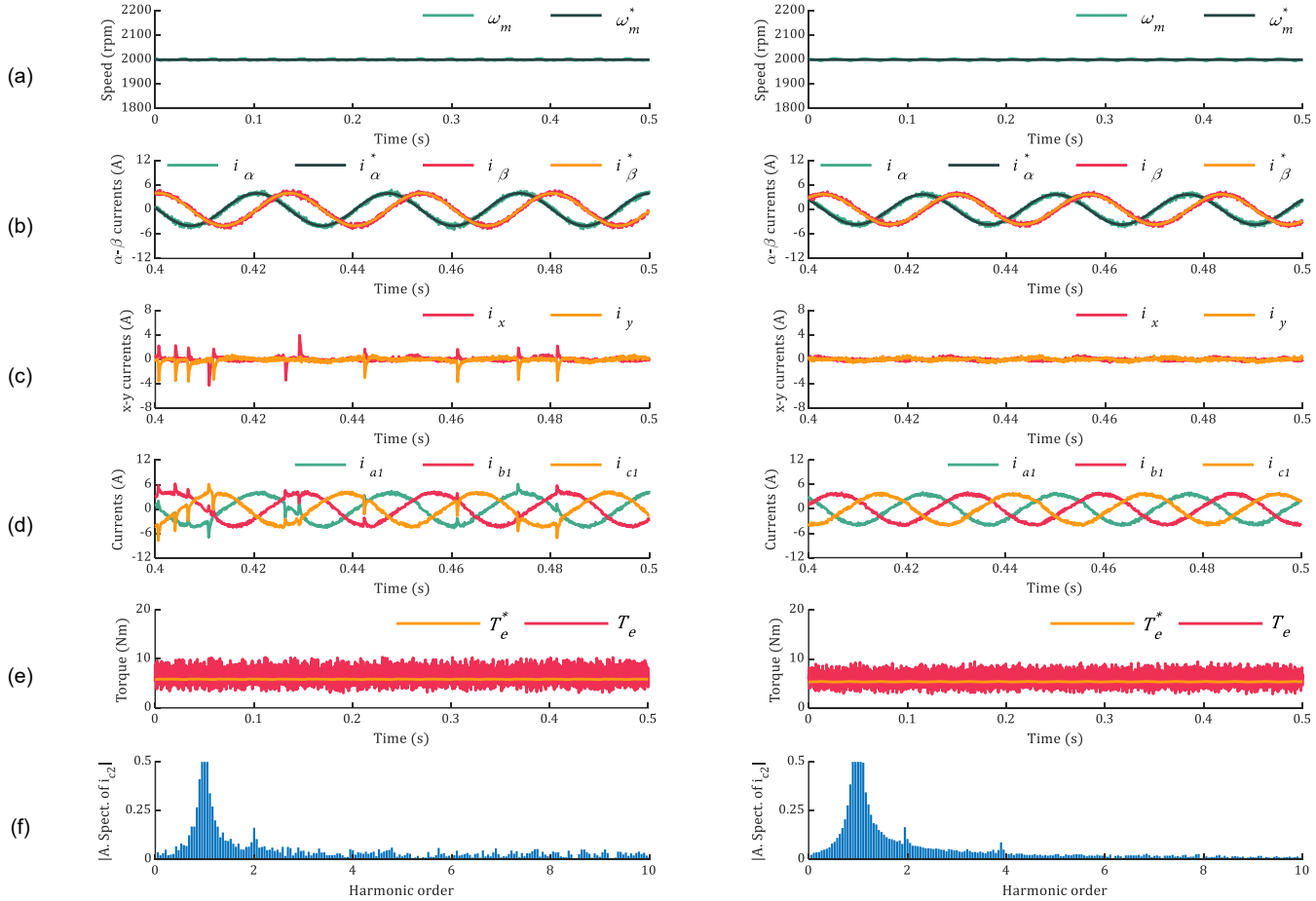


Fig. 11. Test 1: FCS-MPC#1 (left column) and FCS-MPC#2 (right column) regulating S6 IM. From top to bottom: (a) motor speed, (b) $\alpha$-$\beta$ currents, (c) $x$-$y$ currents, (d) zoom of the set 1 of phase currents, (e) estimated electrical torque and (f) harmonic spectrum of the phase current $c_2$. Test condition: reference speed $\omega_m^* = 2000\ rpm$; load torque: $T_e^* = 5.8\ Nm$.

FCS-MPC#2 (S6),both of them using large and null voltage vectors as control actions. The reference speed is established at 500 rpm as shown in Fig. 14a, where the left plots include the results of the asymmetrical IM and the right plots illustrate the symmetrical shifting behavior. The currents components related to the flux/torque production (i.e., $\alpha$-$\beta$ currents) present a slightly lower ripple in the case of the symmetrical machine (see Fig. 14b), since FCS-MPC#2 is only focused on the regulation of these components. As expected, the better result of the symmetrical IM is further accentuated in the secondary subspace, where FCS-MPC#2 can achieve $x$-$y$ currents that are close to zero (Fig. 14c). The waveform of phase currents depends on the regulation performance of the two orthogonal planes and, therefore, the stator currents present an inadmissible harmonic ratio for the A6 motor (Fig. 14d and Table III). In the S6, the lower $x$-$y$ distortion (Fig. 14f) is obtained thanks to the suitable localization of large voltage vectors, consequently a reduced $\overline{rms}$ is obtained (Table III). On the other hand, thanks to the percentage of application of the null voltage vector the switching frequency is also minimized (see Table III) with the symmetrical solution.

The preferable performance of symmetrical distribution for direct controllers has been confirmed over the entire operating range.

## V. Conclusions

Symmetrical multiphase machines with an even number of phases present an interesting feature to reduce the harmonic injection. Their $\alpha$-$\beta$ large voltage vectors show a null production in the secondary subspaces if harmonics of even order are mapped into these planes. This fact allows identifying ideal control actions when direct controllers, such as FCS-MPC, are employed. A maximum flux/torque production can be achieved with null injection of voltage harmonics caused by the $x$-$y$ components. Indeed, for the same test conditions, the tested S6 machine achieves a significant improvement in the total current harmonic distortion, with a reduction of 72.04% over the asymmetrical configuration. Based on the presented results, the symmetrical stator shifting can be regarded as the preferable stator distribution in electric machines to implement direct control schemes when the space harmonics can be neglected.

TABLE II
TEST 3 Conditions & Quality Indexes

| Parameter description | Asymmetrical | Symmetrical |
|---|---|---|
| Null voltage vectors usage (%) | 11.69 | 35.09 |
| $\bar{f}_{sw}$(Hz) | 1678 | 2104 |
| $\overline{THD}$(%) | 53.08 | 14.84 |
| $\overline{rms}$(A) | 3.30 | 2.53 |

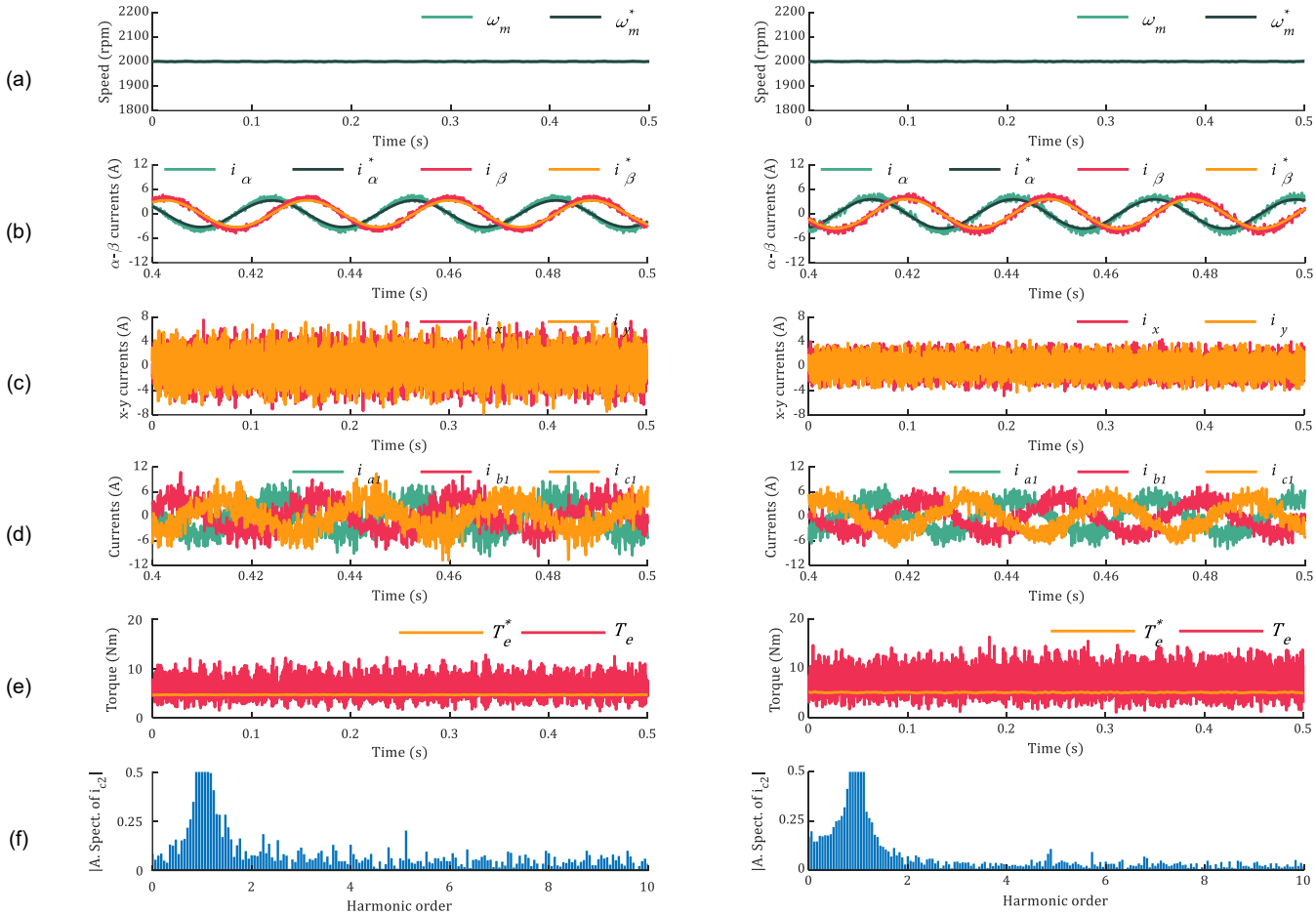


Fig. 12. Test 2: High-speed conditions for asymmetrical six-phase induction machine when FCS-MPC#1 using all the available voltage vectors (left column) and FCS-MPC#1 using large voltage vectors (right column) are employed. From top to bottom: (a) motor speed, (b) $\alpha$-$\beta$ currents, (c) $x$-$y$ currents, (d) zoom of the set 1 of phase currents, (e) estimated electrical torque and (f) harmonic spectrum of the phase current $c_2$. Test condition: reference speed $\omega_m^* = 2000\,rpm$; load torque: $T_e^* = 5.8\,Nm$.

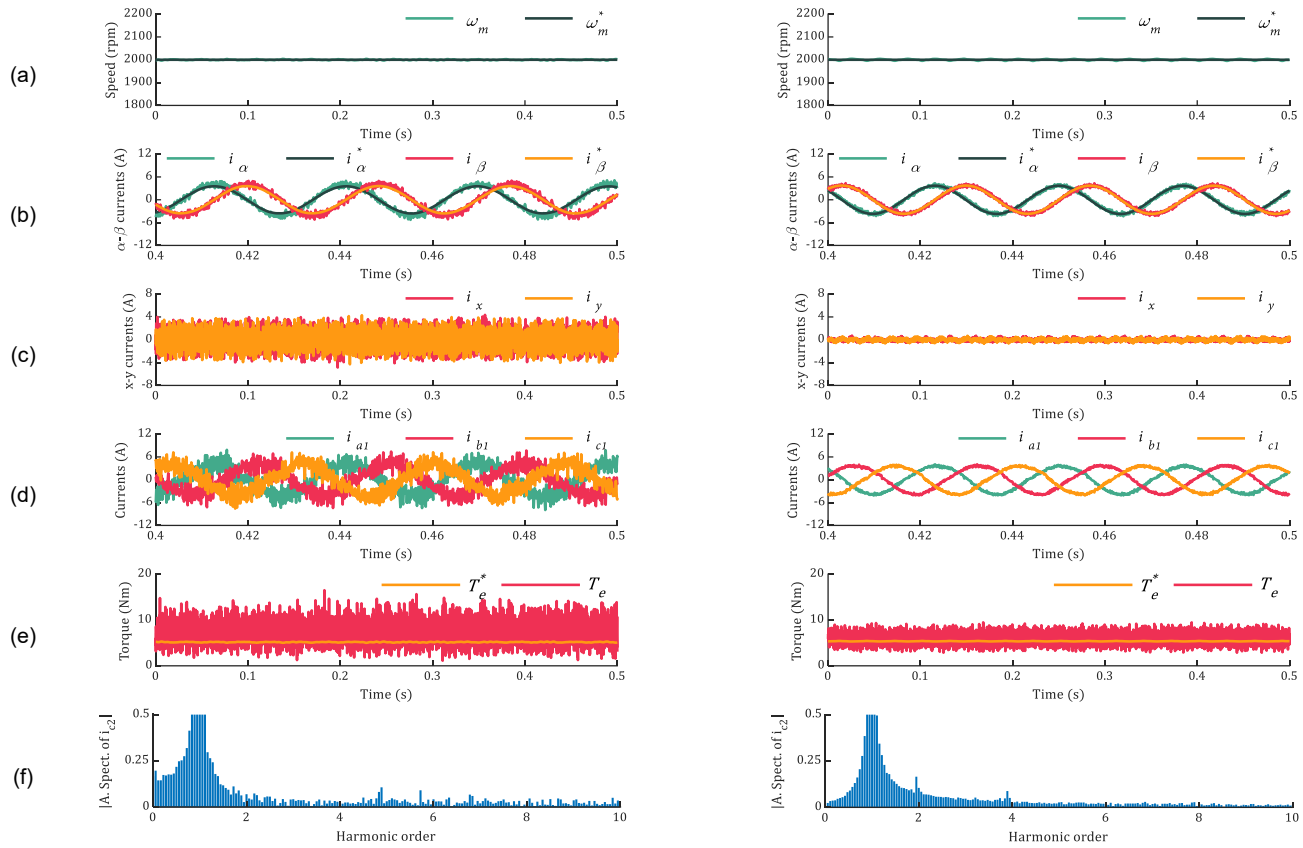


Fig. 13. Test 3: High-speed conditions for asymmetrical (left column) and symmetrical (right column) six-phase IM. From top to bottom: (a) motor speed, (b) $\alpha$-$\beta$ currents, (c) $x$-$y$ currents, (d) zoom of the set 1 of phase currents, (e) estimated electrical torque and (f) harmonic spectrum of the phase current $c_2$. Test condition: reference speed $\omega_m^* = 2000\ rpm$; load torque: $T_e^* = 5.8\ Nm$.

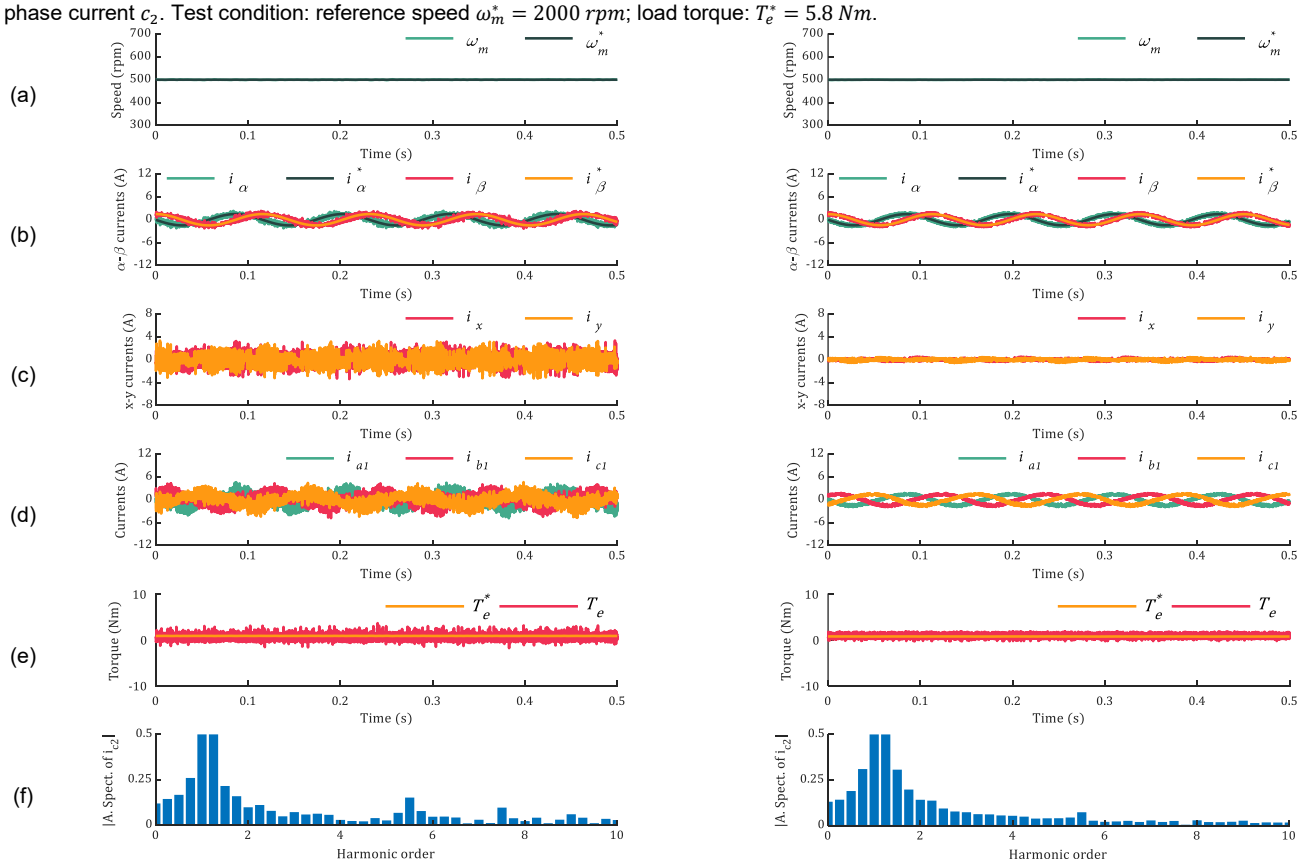


Fig. 14. Test 4: Low-speed conditions for asymmetrical (left column) and symmetrical (right column) six-phase IM. From top to bottom: (a) motor speed, (b) $\alpha$-$\beta$ currents, (c) $x$-$y$ currents, (d) zoom of the set 1 of phase currents, (e) estimated electrical torque and (f) harmonic spectrum of phase current $c_2$. Test condition: reference speed $\omega_m^* = 500\ rpm$; load torque: $T_e^* = 0.8\ Nm$.

TABLE III
TEST 4 CONDITIONS & QUALITY INDEXES

| Parameter description | Asymmetrical | Symmetrical |
|---|---|---|
| Null voltage vectors usage (%) | 50.31 | 69.30 |
| $\bar{f}_{sw}$ (Hz) | 2181 | 1449 |
| $\overline{THD}$(%) | 111.35 | 30.94 |
| $\overline{rms}$(A) | 1.48 | 1.08 |

## REFERENCES


[1] I. Boldea, "Control issues in adjustable speed drives," *IEEE Ind. Electron. Mag.*, vol. 2, no. 3, pp. 32-50, 2008.

[2] E. Levi, "Multiphase electric machines for variable-speed applications," *IEEE Trans. Ind. Electron.*, vol. 55, no. 5, pp. 1893-1909, 2008.

[3] E. Levi, "Advances in converter control and innovative exploitation of additional degrees of freedom for multiphase machines," *IEEE Trans. Ind. Electron.*, vol. 63, no. 1, pp. 433-448, 2016.

[4] I. González-Prieto, I. Zoric, M. J. Duran and E. Levi, "Constrained model predictive control in nine-phase induction motor drives," *IEEE Trans. Energy Convers.*, vol. 34, no. 4, pp. 1881-1889, 2019.

[5] J. K. Pandit, M. V. Aware, R. Nemade and Y. Tatte, "Simplified implementation of synthetic vectors for DTC of asymmetric six-phase induction motor drives," *IEEE Trans. Ind. Appl.*, vol. 54, no. 3, pp. 2306-2318, 2018.

[6] L. Shao, W. Hua, N. Dai, M. Tong and M. Cheng, "Mathematical modeling of a 12-phase flux-switching permanent-magnet machine for wind power generation," *IEEE Trans. Ind. Electron.*, vol. 63, no. 1, pp. 504-516, 2016.

[7] R. Bojoi, M. Lazzari, F. Profumo and A. Tenconi "Digital field-oriented control for dual three-phase induction motor drives," *IEEE Trans. Ind. Appl*., vol. 39, no. 3, pp. 752-760, 2003.

[8] H.S. Che, E. Levi, M. Jones, W.P. Hew and N.A. Rahim, "Current control methods for an asymmetrical six-phase induction motor drive," *IEEE Trans. Power Electron.,* vol 29, no. 1, pp. 407-417, 2014.

[9] R. Bojoi, F. Farina, M. Lazzari, F. Profumo, A. Tenconi, "Analysis of the asymmetrical operation of dual three-phase induction machines," *Proc. IEEE ICEMD*, vol. 1, pp. 429-435, 2003.

[10] A. G. Yepes, J. Doval-Gandoy, F. Baneira and H. A. Toliyat, "Control strategy for dual three-phase machines with two open phases providing minimum loss in the full torque operation range," *IEEE Trans. Power Electron.,* vol. 33, no. 12, pp. 10044-10050, 2018.

[11] D.Dujic, A. Iqbal and E. Levi, "A space vector PWM technique for symmetrical six-phase voltage source inverters," *EPE Journal*, vol. 17, no. 1, pp. 24-32, 2015.

[12] D. Glose, "Continuous space vector modulation for symmetrical six-phase drives," *IEEE Trans. Power Electron.*, vol. 31, no. 5, pp.3837-3848, 2016.

[13] R. Kianinezhad, B. Nahid, F. Betin and G. Capolino, "Multi-vector SVM: a new approach to space vector modulation control for six-phase induction machines," *Proc. IEEE IECON 2005*, Raleigh, NC, 2005.

[14] R. H. Nelson and P. C. Krause, "Induction machine analysis for arbitrary displacement between multiple winding sets," *IEEE Trans. Power App. Syst.*, vol. PAS-93, no. 3, pp. 841-848, 1974.

[15] E. Levi, R. Bojoi, F. Profumo, H. A. Toliyat and S. Williamson, "Multiphase induction motor drives - A technology status review," *IET Electric Power Appl.*, vol. 1, no. 4, pp. 489-516, 2007.

[16] A. S. Abdel-Khalik, M. S. Abdel-Majeed and S. Ahmed, "Effect of winding configuration on six-phase induction machine parameters and performance," *IEEE Access*, vol. 8, pp. 223009-223020, 2020.

[17] W. N. W. A. Munim, M. J. Duran, H. S. Che, M. Bermúdez, I. González-Prieto and N. A. Rahim, "A unified analysis of the fault tolerance capability in six-phase induction motor drives," *IEEE Trans. Power Electron.*, vol. 32, no. 10, pp. 7824-7836, 2017.

[18] A. Gonzalez-Prieto, I. Gonzalez-Prieto and M. J. Duran, "Smart voltage vectors for model predictive control of six-phase electric drives," *IEEE Trans. Ind. Electron.*, vol. 68, no. 10, pp. 9024-9035, 2021.

[19] J. J. Aciego, I. Gonzalez-Prieto, M. J. Duran, M. Bermudez and P. Salas-Biedma, "Model predictive control based on dynamic voltage vectors for six-phase induction machines," *IEEE Trans. Emerg. Sel. Topics Power Electron.*, vol. 9, no. 3, pp. 2710-2722, 2021.

[20] Y. Luo and C. Liu, "Multi-Vectors based model predictive torque control for a six-phase PMSM motor with fixed switching frequency," *IEEE Trans. Energy Convers.,* vol. 34, no. 3, pp. 1369-1379, 2019.

[21] P. F. C. Gonçalves, S. M. A. Cruz, and A. M. S. Mendes, "Fixed and variable amplitude virtual vectors for model predictive control of six-phase PMSMS with single neutral configuration," *Proc. IEEE Int. Conf. Ind. Tech.,* Melbourne, Australia, 2019.

[22] H. A. Young, M. A. Perez, J. Rodriguez and H. Abu-Rub, "Assessing finite-control-set model predictive control: A comparison with a linear current controller in two-level voltage source inverters," *IEEE Ind. Electron. Mag.*, vol. 8, no. 1, pp. 44-52, 2014.

[23] A. Gonzalez-Prieto, I. Gonzalez-Prieto, A. Yepes, M. J. Duran and J. Doval-Gandoy, "Symmetrical six-phase induction machines: A solution for multiphase direct control strategies," *Proc. IEEE Int. Conf. Ind. Tech.*, Valencia, Spain, 2021.

[24] Yifan Zhao and T. A. Lipo, "Space vector PWM control of dual three-phase induction machine using vector space decomposition," *IEEE Trans. Ind. Appl.*, vol. 31, no. 5, pp. 1100-1109, 1995.

[25] I. Zoric, M. Jones and E. Levi, "Vector space decomposition algorithm for asymmetrical multiphase machines," *2017 Int. Symposium Power Electron.* (Ee2017), Novi Sad, pp. 1-6, 2017.

[26] J. Malvar et al., "Graphical Diagram for Subspace and Sequence Identification of Time Harmonics in Symmetrical Multiphase Machines," *IEEE Trans. Ind. Electron.*, vol. 61, no. 1, pp. 29-42, 2014.

[27] B. Chen, J. Lv and X. Jiang, "Simplified model predictive control of a twelve-phase permanent magnet synchronous motor," *45th Annual Conf. of IEEE IECON 2019*, Lisbon, Portugal, 2019, pp. 1345-1350.

[28] M.J. Duran, I. Gonzalez-Prieto and A. Gonzalez-Prieto, "Large virtual voltage vectors for direct controllers in six-phase electric drives," *Int. J. of Electr. Power Energy Syst.,* vol. 125, 2021.

[29] A. Yepes et al. "Parameter identification of multiphase induction machines with distributed windings-part 1: sinusoidal excitation methods," *IEEE Trans. Energy Conv*., vol. 27, no. 4, pp. 1056-1066, 2012.


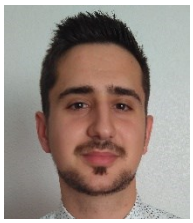

**Angel González-Prieto** was born in Malaga, Spain, in 1993. He received the University and M. Sc. degrees in Industrial Engineering from the University of Málaga, Málaga, Spain, in 2017 and 2019, respectively. He is currently developing his Ph.D. in Electric Energy Systems Program at the University of Malaga. His research interests include multiphase machines and renewable energy conversion system.

**Ignacio González-Prieto** was born in Malaga, Spain, in 1987. He received the Industrial Engineer and M.Sc. degrees in Fluid Mechanics from the University of Malaga, Malaga, Spain, in 2012 and 2013, respectively, and the Ph.D. degree in electronic engineering from the University of Seville, Sevilla, Spain, in 2016. His research interests include multiphase machines, wind energy systems, and electrical vehicles.

**Alejandro G. Yepes** (Senior Member, IEEE) received the M.Sc. and Ph.D. degrees in electrical engineering from Universidade de Vigo, Vigo, Spain, in 2009 and 2011, respectively.
Since 2008, he has been working with the Applied Power Electronics Technology Research Group, Universidade de Vigo. His research interests are in the areas of ac power conversion, with special focus, currently, on multiphase drives.

**Mario J. Duran** was born in Bilbao, Spain, in 1975. He received the M.Sc. and Ph.D. degrees in electrical engineering from the University of Malaga, Malaga, in 1999 and 2003, respectively. He is currently a Full Professor in the Department of Electrical Engineering, University of Malaga. His research interests include modeling and ´ control of multiphase drives and renewable energies conversion systems.

**Jesus Doval-Gandoy** received the M.Sc. and Ph.D. degrees in electrical engineering from the Polytechnic University of Madrid, Madrid, Spain, and from Universidade de Vigo, Vigo, Spain, in 1991 and 1999, respectively. He is a Professor and the Head of the Applied Power Electronics Technology Research Group (APET), Universidade de Vigo. His research interests are in the areas of ac power conversion.